RESEARCH ARTICLE

Identification of SIRT3 modulating compounds in deep-sea fungi metabolites: Insights from molecular docking and MD simulations

Abdullah R. Alanzi*, **Bayan Abdullah Alhaidhal**, **Raghad Mohammad Aloatibi**

Department of Pharmacognosy, College of Pharmacy, King Saud University, Riyadh, Saudi Arabia

* aralonazi@ksu.edu.sa

Abstract

SIRT3, a crucial deacetylase that plays a key role in regulating mitochondrial acetylation, is tightly linked to metabolic processes and is essential for the maintenance of eukaryotic life. SIRT3 is a potential therapeutic target due to its key role in various diseases, including ageing, heart disease, cancer, and metabolic disorders. In this work, we aimed to identify potential SIRT3 inhibitors from the deep-sea fungal metabolites by employing molecular docking and ADMET analysis. Based on the binding affinities, ten compounds were selected whose docking scores were in the range of -9.693 to -8.327 kcal/mol. Further, four compounds Penipanoid C, Penicillactam, Quinolonimide, and Brevianamide R were selected based on the ADMET properties and subjected to Molecular dynamics simulations to assess the stability of these molecules with target. The stability analysis indicated that the selected compounds could act as lead compounds during *in vitro* assays to advance these drug candidates towards clinical drug development.

1. Introduction

Sirtuins are a family of protein deacetylases that depend on NAD + for their activity, and although they typically appear in only one or two forms in bacteria and archaea, they are present in seven distinct forms (SIRT1–7) in mammals [1–3]. These enzymes may be divided into five sub classes according to the conserved catalytic core domain. SIRT1, SIRT2, and SIRT3 are class I proteins that are identified by their high deacetylase activity levels. SIRT4 is a Class II enzyme that functions as an ADP-ribosyl transferase in mitochondria. While, SIRT5 is categorized as Class III, and SIRT6 and SIRT7 as Class IV [4,5].

SIRT3 is mostly found in the mitochondrial matrix and is essential for controlling various aspects of mitochondrial metabolism [6]. Its actions include the regulation of the following processes: the electron transport chain (ETC), oxidative phosphorylation (OXPHOS), fatty acid oxidation, amino acid metabolism, mitochondrial dynamics,

detoxification of reactive oxygen species (ROS), urea cycle, tricarboxylic acid (TCA) cycle, and mitochondrial unfolded protein response (UPR) [7,8]. SIRT3 protein has been found in the brain, kidney, liver, heart, and other tissues with high mitochondrial concentrations [9,10]. The maintenance of mitochondrial function in these tissues is dependent on acetylation modifications mediated by SIRT3. The importance of mitochondria may be attributed to their vital functions in energy production, metabolism, intracellular signaling, and apoptosis. This is particularly true in tissues with high metabolic activity, which are more vulnerable to mitochondrial dysfunction [11]. Studies have shown the involvement of SIRT3 in the regulation of ageing, neurological disorders, cardiovascular disorders, hepatic disorders, kidney disorders, and further metabolic irregularities. Moreover, studies have shown its intriguing dual involvement in the development of cancer [10]. It also regulates the mitochondrial protein acetylation during renal fibrosis [12]. As a result, SIRT3 is a promising target for therapeutic intervention in a variety of human diseases [13]. Preclinical research on different small-molecule drugs that target SIRT3 has produced encouraging findings [14,15].

Currently, there is no widely recognized strong inhibitor or activator of SIRT3 suitable for therapeutic treatments. Still, a number of small-molecule compounds have been found that may have therapeutic value [2]. In particular, the well-known SIRT3 activator honokiol shows promise for treating illnesses linked to inflammation, cardiac problems, cancer, and metabolic issues. It's crucial to remember, that SIRT3 activation is not the only factor contributing to Honokiol's positive benefits [15]. Recent work by Upadhyay et al. indicates that honokiol stimulates SIRT3 through a non-allosteric mechanism. By extending the earlier findings of Guan et al., this work advances our knowledge of the molecular mechanisms behind Honokiol's SIRT3 activation [16]. Currently, 3-TYP and other SIRT3 inhibitors are mostly used as research purpose and are not yet utilized in therapeutic contexts [2,17]. This emphasizes how difficult it is yet to create strong SIRT3 activators or inhibitors for medical applications. Using scientific drug design techniques becomes imperative. Therefore, the purpose of this study was to screen deep-sea fungal metabolites to find new inhibitors that target SIRT3. The goal of the study is to find molecules that may open the door for the creation of therapeutic medicines that target pathways connected to SIRT3.

2. Methodology

2.1. Preparation of ligands

The structures of deep-sea fungal metabolites were downloaded from PubChem (https://pubchem.ncbi.nlm.nih.gov/). The Maestro LigPrep tool was utilized to prepare the structures of the phytochemicals [18]. Thirty-two conformers were produced for each ligand after the geometry of each ligand was optimized to assure accuracy. To reduce the compounds' energy, the OPLS_2005 force field was used [19].

2.2. Molecular docking

This study focuses on investigating the molecular interactions between deep-sea fungi metabolites and the SIRT3 protein to identify potential compounds with

inhibitory activity. The Protein Data Bank provided the crystal structure of SIRT3 (PDB ID: 4JSR). The SIRT3 protein structure was processed for docking using the Protein Preparation Wizard in Schrodinger Maestro [20]. Different steps were conducted, including the addition of hydrogens, the formation of disulfide bonds, the formation of zero-order bonds to metals, and the assignment of bond orders. PROPKA was used to eliminate extra ligands and water molecules and optimize hydrogen bonds at pH 7.0 [21,22]. Finally, the protein's energy was minimized using the OPLS_2005 force field [19]. A 3D grid was created at the binding site coordinates (X = 23.18, Y = 45.84, Z = -2.01) after the protein was prepared to aid in site-specific docking. Next, using the Glide docking module in SP (Standard Precision) mode, the prepared ligands were docked against SIRT3 [23]. Following analysis of the docked ligands, the Glide scores were used to determine the selection. Moreover, docking results were validated by re-docking procedure.

2.3. Toxicity analysis

The drug erosion is linked to toxicity concerns and suboptimal pharmacokinetics of the compounds [24]. To address this, the ADMET profiles were analyzed to evaluate the toxicity risks of drug candidates [25]. This predictive approach also helps in evaluating the likelihood of lead compounds becoming viable oral drugs. In this study, we used OSIRIS Property Explorer tool [26] to predict the ADMET characteristics of the most promising compounds. We assessed several pharmacokinetic properties, including molecular weight (MW), solubility (log S), logP, TPSA, and drug-likeness and score. Additionally, we scrutinized the compounds for potential toxicity consequences, encompassing tumorigenic, mutagenic, irritating, and reproductive concerns.

2.4. Molecular dynamics simulation and post MD analyses

The complexes were analyzed for protein conformation and ligand stability by running a simulation of 100 ns by using Desmond [27]. The systems were solvated by placing them in an orthorhombic box of 10 Å, filled with TIP3P water model [28]. To replicate physiological conditions, counter ions were added for neutralization, and 0.15 M NaCl salt was incorporated. The temperature and pressure of the system was set to 300K and 1 ATM respectively by using NPT ensemble. After a relaxation phase, the production run was started to record the trajectories after 50 ps time interval. The simulation interaction diagram module of Desmond was used to analyze the trajectories. In MD simulations with Desmond, we employed the standard Desmond relaxation protocol prior to the production run. This protocol involved an initial energy minimization followed by a short equilibration phase of 1 ns during which position restraints (using a force constant of 25 kcal/mol/Å²) were applied to the heavy atoms of the protein. This equilibration step allowed the solvent and ions to relax around the restrained protein-ligand complex. MMGBSA analysis was performed to calculate binding free energy calculations as well as hydrogen bonding and radius of gyration analyses were performed. PCA and 2D Free Energy Surface analyses was carried out to assess conformational variance and stability. Per-residue energy decomposition was carried out to estimate the individual binding free energy contribution of SIRT3 binding site residues to the stabilization and affinity of studied compounds.

3. Results

3.1. Molecular docking

The compounds identified through virtual screening were prepared, and a docking study was subsequently performed on the SIRT3 protein [29]. The binding affinities of all docked compounds were analyzed and then top ten compounds with binding affinities ranging from -9.693 to -8.327 kcal/mol were selected for further analysis (Table 1). The docking scores of the selected compounds suggested that these have potential for inhibiting the function of the SIRT3 protein. These findings provide valuable insights into the possibility of these compounds interacting effectively with the SIRT3 binding site, thereby warranting additional investigation into their inhibitory potential. Moreover, to further validate the docking analysis,

Table 1. The glide scores of the docked compounds against SIRT3 protein.

Sr.	Compounds	PubChem CIDs	Glide score (kcal/mol)
1	Cyclopiamide D	122218854	−9.693
2	Penilumamide K	156580691	−9.5
3	Coccoquinone A	132512004	−9.09
4	Penipanoid C	136171438	−8.86
5	Penicillactam	57337607	−8.827
6	Quinolonimide	11492325	−8.798
7	Prenylterphenyllin	23630784	−8.751
8	Brevianamide R	49831335	−8.553
9	Butanolide A	156581743	−8.494
10	Dichotocejpin C	139583288	−8.327

https://doi.org/10.1371/journal.pone.0323107.t001

a re-docking procedure was performed. Interestingly, the both the native and redocked ligands' conformation and pose was somewhat highly similar in the binding site of the SIRT3 receptor validating the initial docking procedure [Fig 1].

3.2. ADMET analysis

The ADMET and toxicity risks profiles of the selected compounds were analyzed by OSIRIS Property Explorer tool, and it was observed that the predicted values were in the acceptable range (Table 2). The molecular weight plays a vital role in the distribution of a compound within cells, with lower-weight compounds generally able to distribute more easily throughout the body compared to those with higher weights [30]. To address this, a threshold of 500 g/mol was established, and all selected compounds fell within this range. cLogP determines the hydrophilicity of compound, a value of cLogP > 5 indicates poor absorption. The selected hits had cLogP values less than 5, indicating good absorption of compounds. The TPSA relates with the hydrogen bonding of a compound and is a good predictor of bioavailability [31]. TPSA < 160 Å^2 shows that the compound will have good oral bioavailability [32]. The hits had TPSA values in the range of 66.58 to 190.9 Å^2. Solubility is also a crucial factor in pharmacokinetics, influencing both the absorption and distribution of a compound. It is typically quantified as the logarithm of the solubility, expressed in mol/dm^3. This measurement helps to assess how easily a compound dissolves in a solvent, which is vital for its effective utilization in the body and its overall pharmacokinetic profile. The drug score is a comprehensive measure that combines several factors such as, cLogP, logS, molecular weight, and toxicity risk into a single, easy-to-understand number. This score is used to evaluate a compound's overall potential to become a drug. A higher drug score indicates a greater likelihood that the compound could be a viable drug candidate. In essence, the higher the drug score value, the more likely the compound is to be considered for further drug development [33]. Furthermore, the toxicity profile of compounds was evaluated, and it was observed that the compounds did not show toxicity tendencies except for **Cyclopiamide D, Coccoquinone A, Butanolide A,** and **Dichotocejpin C.** Based on the pharmacokinetic and toxicity profiles, 4 compounds, i.e., **Penipanoid C, Penicillactam, Quinolonimide**, and **Brevianamide R** were selected for molecular interactions analysis.

3.3. Molecular interactions analysis

The docked poses of the selected compounds were analyzed by Discovery Studio client tool to find the molecular interactions. The molecular interactions mainly involved hydrogen bonding, van der Waal interactions, pi-pi stacking, pi-sigma interactions, and alkyl (hydrophobic) interactions. The molecular interactions of each candidate compounds help in determining the binding affinities. Especially, the hydrogen bonds among ligand and protein atoms play an important role in the strength of protein-ligand complex [34]. **Penipanoid C** formed one van der Waal interaction with Ile291, two hydrogen
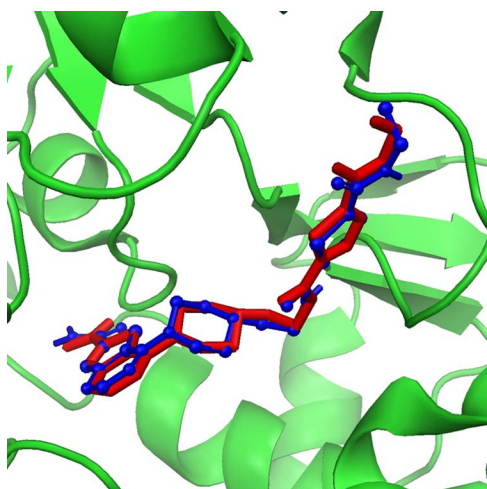
Fig 1. Redocking of the ligand, native ligand is represented by red and redocked ligand is represented by blue colors.

Table 2. The ADMET and Toxicity risks analysis of top ten compounds.

Compounds	Pharmacokinetic Properties						Toxicity Risks			
	MW	cLogP	TPSA	LogS	Drug likeness	Drug score	Mutagenic	Tumorigenic	Irritant	Reproductive effect
Cyclopiamide D	336	2.28	83.55	−4.49	−3.52	0.08	High	High	High	Passed
Penilumamide K	442	−1.16	190.9	−3	2.72	0.76	Passed	Passed	Passed	Passed
Coccoquinone A	428	2.71	158.4	−4.78	−2.09	0.13	High	Passed	High	Passed
Penipanoid C	**266**	**1.0**	**78.76**	**−3.06**	**4.35**	**0.9**	**Passed**	**Passed**	**Passed**	**Passed**
Penicillactam	**395**	**0.02**	**133.8**	**−3.59**	**6.56**	**0.8**	**Passed**	**Passed**	**Passed**	**Passed**
Quinolonimide	**228**	**−0.06**	**66.58**	**66.48**	**6.25**	**0.95**	**Passed**	**Passed**	**Passed**	**Passed**
Prenylterphenyllin	406	5.82	79.15	−5.87	−0.23	0.27	Passed	Passed	Passed	Passed
Brevianamide R	**379**	**3.03**	**74.43**	**−4.17**	**1.96**	**0.68**	**Passed**	**Passed**	**Passed**	**Passed**
Butanolide A	254	1.85	66.76	−2.53	−10.55	0.28	Passed	Passed	High	Passed
Dichotocejpin C	262	−0.63	81.08	−1.17	6.65	0.35	Passed	High	High	Passed

bonds with Val292, Phe157, two Pi-Pi stacked interactions with His248, Phe180 and two alkyl interactions with Ile230, Ala146 (**Fig 2a**). **Penicillactam** formed five van der Waal interactions with Ile154, Pro155, Arg158, Gln228, Ile230, three hydrogen bonds with Phe157, Asn229, Tyr165, Pi-Sigma interaction with Ala146, and one alkyl interaction with His248 (**Fig 2b**). Similarly, **Quinolonimide** made two van der Waal interactions with Phe294, Ile154, two hydrogen bonds with Ile230, Phe157, two carbon hydrogen bonds with Gln228, Asp156, and two alkyl interactions with His248, Ala146 (**Fig 2c**). Lastly, **Brevianamide R** made one Pi-Sigma interaction with His248, two hydrogen bonds with Val292, Tyr165, one Pi-Pi stacked interaction with Phe294 and six alkyl interactions with Ile230, Ile291, Phe180, Phe157, Arg158, Ala146 (**Fig 2d**). The interactions of the remaining compounds are displayed in Table 3.

3.4. Analysis of plausible binding modes

The plausible binding modes of the selected compounds were observed by alignment on co-crystal ligand. This alignment showed that the docked poses of the hits occupied the same space in binding sites of the SIRT3 as occupied by co-crystal ligand (**Fig 3**). As a result, the plausible binding modes of the docked hits were evaluated for stability through Molecular
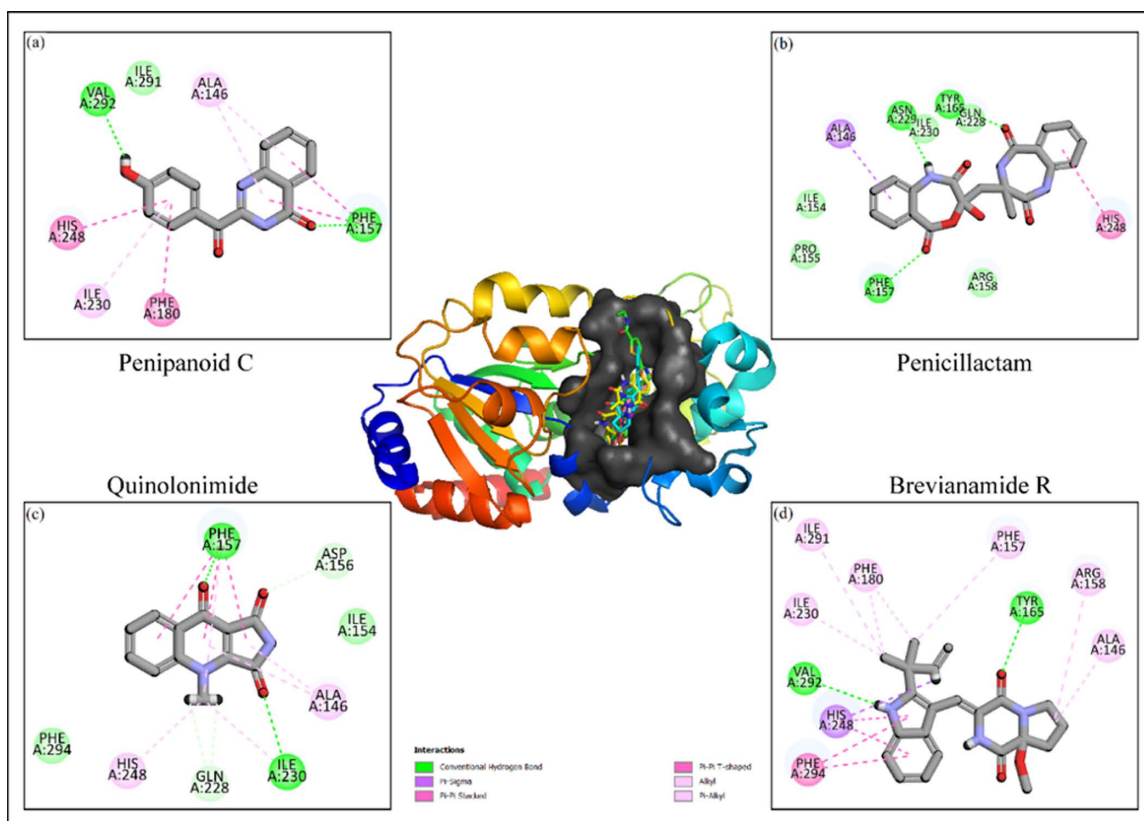
Fig 2. The 2D molecular interactions of the selected compounds based on the pharmacokinetic and toxicity profiles with the SIRT3 receptor with diversity of bond formations indication a stabilization of ligands into receptor's active pocket.

https://doi.org/10.1371/journal.pone.0323107.g002

Dynamics (MD) simulations. In addition, key interactions such as hydrogen bonds with critical residues, e.g., Phe157, Val292, TYR165 and His248 and hydrophobic contacts were observed in the docked poses, mirroring those found in the co-crystallized structure. These observations support the plausibility of the binding modes predicted by docking, suggesting that the hit compounds engage the receptor in a manner consistent with known SIRT3 inhibition mechanisms. The stability of these binding orientations was subsequently assessed through molecular dynamics simulations, which further confirmed that the compounds maintained their key interactions and overall binding conformations throughout the simulation period.

3.5. MD simulation

3.5.1. RMSD. The root mean square deviation of the Cα atoms was measured to evaluate the structural changes of the complexes the RMSD values were calculated across the simulation [35,36]. The **Penipanoid C** complex's RMSD values displayed significant deviations during the first 20 ns, reaching a maximum value of 3.6 Å. However, after 20 ns, stability was reached in the 2.4 Å range, which was maintained throughout the simulation. The RMSD of ligand atoms was also aligned on protein atoms after 20 ns (**Fig 4a**). The RMSD of **Penicillactam** maintained the RMSD value of 2.1 Å at the start and remained in this range throughout the simulation., while the RMSD of ligand atoms aligned on protein atoms after 20 ns (**Fig 4b**). In the case of **Quinolonimide** complex, the RMSD of protein carbon-alpha atoms gradually increased to 2.8 Å at 10 ns and then maintained this range till 60 ns. The simulation ended with the RMSD staying in the

Table 3. The molecular interactions of the selected compounds with SIRT3 protein.

Sr.	Compounds	Interactions
1	Cyclopiamide D	**Van der Waal:** Ala146, Tyr165, Gln228, Ile154, Ser149 **Hydrogen Bond:** Phe157, Ile230, Val292 **Alkyl:** His248, Phe180
2	Penilumamide K	**Van der Waal:** Tyr165, Asn229 **Hydrogen Bond:** Val292, Ile230, Phe157 **Pi-Sigma:** Ala146 **Alkyl:** His248, Ile291
3	Coccoquinone A	**Van der Waal:** His248, Val292, Phe294, Phe180 **Hydrogen Bond:** Gln228, Ile230, Ile154, Phe157, Tyr165 **Alkyl:** Ala146
4	Penipanoid C	**Van der Waal:** Ile291 **Hydrogen Bond:** Val292, Phe157 **Pi-Pi Stacked:** His248, Phe180 **Alkyl:** Ile230, Ala146
5	Penicillactam	**Van der Waal:** Ile154, Pro155, Arg158, Gln228, Ile230 **Hydrogen Bond:** Phe157, Asn229, Tyr165 **Pi-Sigma:** Ala146 **Alkyl:** His248
6	Quinolonimide	**Van der Waal:** Phe294, Ile154 **Hydrogen Bond:** Ile230, Phe157 **Carbon Hydrogen Bond:** Gln228, Asp156 **Alkyl:** His248, Ala146
7	Prenylterphenyllin	**Hydrogen Bond:** Phe293, Glu296, Gly295, Phe157 **Carbon Hydrogen Bond:** Phe180, Val292 **Alkyl:** Phe294, His248, Val324, Ile154, Leu199, Ile230, Ala146
8	Brevianamide R	**Hydrogen Bond:** Val292, Tyr165 **Pi-Sigma:** His248 **Pi-Pi stacked:** Phe294 **Alkyl:** Ile230, Ile291, Phe180, Phe157, Arg158, Ala146
9	Butanolide A	**Van der Waal:** Ile291, Tyr165, Arg158 **Hydrogen Bond:** Val292, Phe157, Phe231, Ile230 **Alkyl:** Phe294, Phe180, His248, Ala146
10	Dichotocejpin C	**Van der Waal:** His248 **Hydrogen Bond:** Phe157, Ile154, Pro155, Ile230, Asn229, Gln228 **Pi-Cation:** Arg158

https://doi.org/10.1371/journal.pone.0323107.t003

range of 3.2 Å after 60 ns. The RMSD of ligand atoms was less than protein atoms after 60 ns (**Fig 4c**). Finally, the RMSD of the **Brevianamide R** complex reached stability in the range of 2.4 at 20 ns and remained there until the end of the simulation. The RMSD of ligand atoms was aligned with RMSD of protein atoms (**Fig 4d**).

3.5.2. RMSF. Root mean square fluctuations (RMSF) values were computed in order to study the dynamic behavior of the proteins while they were bound to the ligands [37,38]. Throughout the simulation, the RMSF values provide information about the mobility and flexibility of specific protein residues. Most protein residues showed only slight changes during the simulation, measuring less than 1.8 Å, based on the estimated RMSF values. This suggests that while the ligands were present, these residues were stable and stiff. In contrast, higher RMSF values (4.8 Å) were found in the protein's loop regions (**Fig 5**). The bulk of residues in the protein-ligand complex maintained a rigid conformation, which indicated overall stability based on the Root Mean Square Fluctuation (RMSF) analysis. The loop regions exhibited higher RMSF values, indicating more prominent fluctuations and dynamic interactions with the ligands.
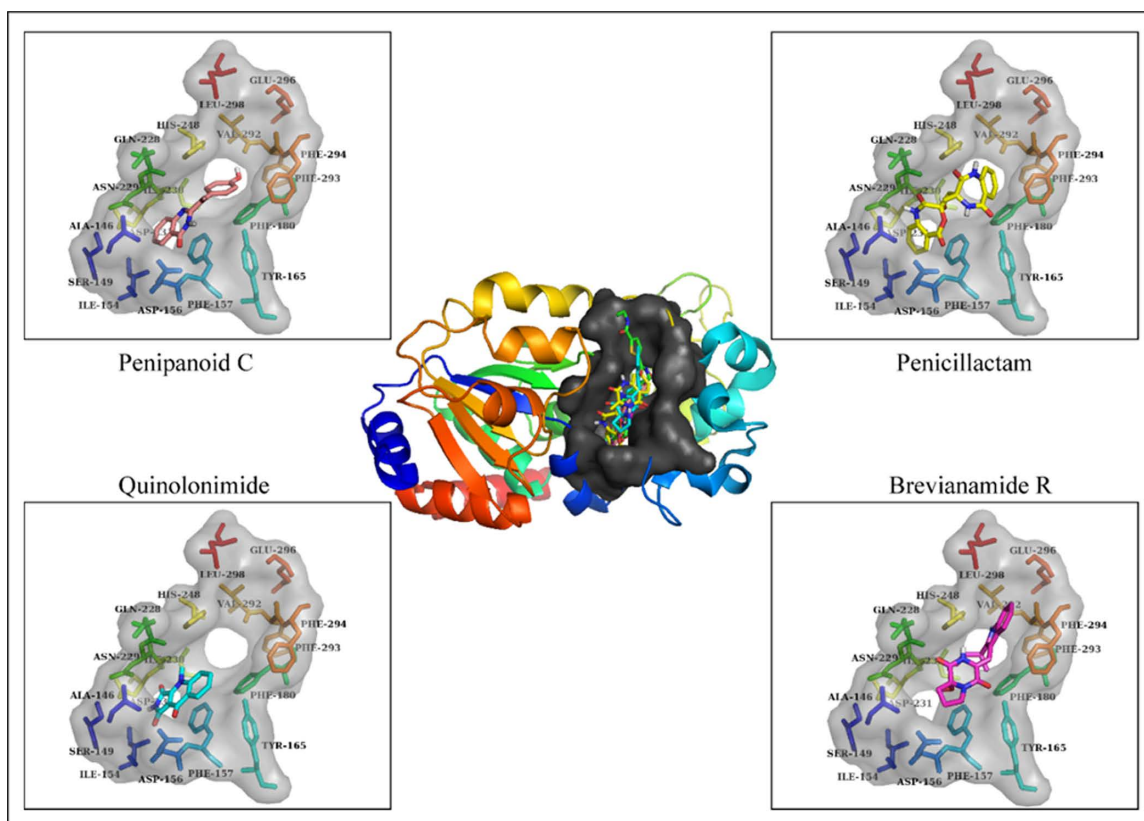
Fig 3. The plausible binding poses of the top four compounds. The binding modes of the compounds with the residues are also shown in sticks.

3.5.3. Protein-ligand interactions. During the simulation, the protein–ligand interfaces were predominantly stabilized by hydrogen bonds, water-mediated bridges, electrostatic forces, and hydrophobic contacts. These contacts play an important role in protein-ligand complex stability during the simulation. There residues involved in hydrogen bonding with **Penipanoid C** were Ser149, Ile154, Phe157, Gln228, Asn229, Ile230, and His248 (**Fig 6a**). In the **Penicillactam** complex, the residues involved in hydrogen bonding were Phe157, Tyr165, Gln228, Ile230, Asp231, and His248 (**Fig 6b**). In the **Quinolonimide** complex, the hydrogen bonding interactions involved Ile230 and Asp231 (**Fig 6c**). Lastly, the hydrogen bonding in **Brevianamide R** was observed in the following residues: Phe157, Leu164, Gln228, and His248 (**Fig 6d**). The hydrogen bonding during MD simulations provides important insights into the specific residues that stabilize the protein-ligand complexes. This information enhances our understanding on how these interactions contribute in the complex stability and binding affinities [39].

3.5.4. Hydrogen bonding analysis. Across the 100 ns simulation, each of the four complexes exhibited characteristic hydrogen-bonding patterns, reflecting both the ligand's affinity for SIRT3 and its dynamic fluctuations. Penipanoid C maintained a fairly consistent range of 13 hydrogen bonds over time, suggesting stable polar interactions within the active site. Penicillactam showed more pronounced fluctuations (spanning 0–4 hydrogen bonds), indicating transient formation and disruption of specific hydrogen-bond contacts. Quinolonimide likewise oscillated between 1–4 hydrogen bonds but displayed occasional spikes of higher bonding, hinting at short-lived yet strong polar contacts. Brevianamide R typically formed 1–3 hydrogen bonds, suggesting it largely retains a stable binding orientation while occasionally sampling alternative configurations (**Fig 7**). Collectively, these results confirm that all four ligands can sustain meaningful
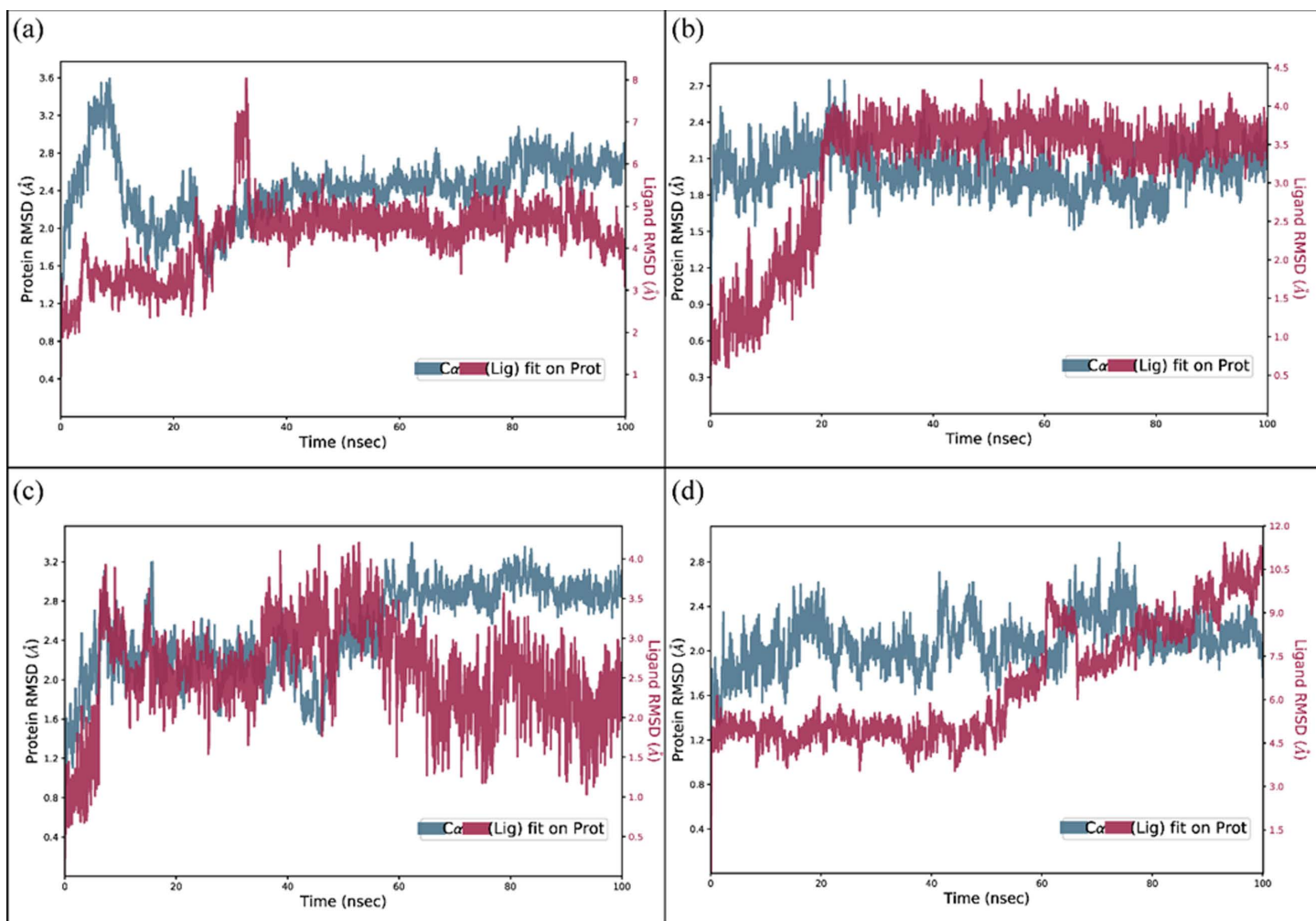
Fig 4. The RMSD plots of the SIRT3 complexes. (a) Penipanoid C with initial deviations at about 20ns but then a good stabilization till the end, (b) Penicillactam with initial deviations at about 20ns but then a good stabilization till the end alongside the protein atoms, (c) Quinolonimide showed gradual increase in RMSD, (d) Brevianamide R.

https://doi.org/10.1371/journal.pone.0323107.g004

hydrogen-bond interactions throughout the simulation, thus reinforcing the notion of stable binding modes inferred from the docking and other MD analyses.

3.5.5. Radius of gyration. For all four SIRT3-ligand complexes, the radius of gyration (Rg) analysis indicates that the overall protein compactness remains remarkably stable over the simulation. In detail, the Rg values for the SIRT3 complexes with Penipanoid C, Penicillactam, Quinolonimide, and Brevianamide R fluctuated within narrow margins (with deviations typically under 0.5 Å), suggesting that none of the ligands induce significant global structural changes in SIRT3. Notably, minor differences in the average Rg values were observed among the complexes, with the Penipanoid C and Brevianamide R complexes showing a slightly more compact protein conformation compared to the Penicillactam and Quinolonimide systems (**Fig 8**). These results confirm that the binding of these deep-sea fungal metabolites does not compromise the structural integrity of SIRT3 during the MD simulation, supporting their potential as stable inhibitors.

3.5.6. PCA and 2D PCA-based free energy surface analysis. For Penipanoid C, the PCA was performed to capture the primary conformational motions of the protein–ligand complex, with the first three eigenvectors explaining roughly 30%
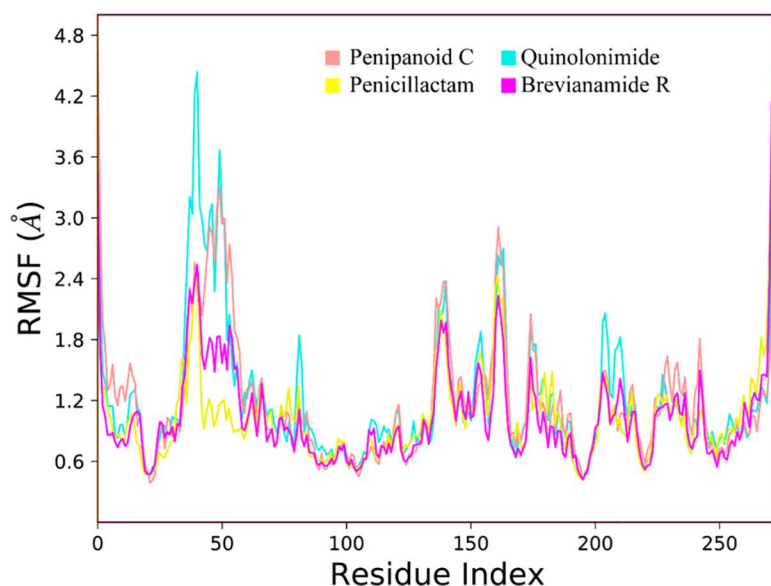
Fig 5. The comparative RMSF plots of the SIRT3 protein in the presence of co-crystal ligand and hit compounds.

https://doi.org/10.1371/journal.pone.0323107.g005

of the total variance. PC1 showed the largest fluctuations, indicating the main direction of motion (**Fig 9A**). Additionally, the 2D PCA-based free energy surface revealed two main conformational clusters: a stable low-energy basin, where Penipanoid C predominantly resides, and a higher-energy region sampled less frequently. This distribution reflects the ligand's intrinsic flexibility while maintaining a largely favorable binding orientation throughout the simulation (**Fig 9B**). The PCA for the Penicillactam-SIRT3 complex revealed that the first few eigenvectors captured the primary motions of the system, with PC1 encompassing the largest fluctuations (**Fig 10A**). In the 2D PCA-based free energy surface, two main conformational clusters emerged: one low-energy basin where Penicillactam remained most of the time, and another higher-energy region visited less frequently (**Fig 10B**). This indicates that Penicillactam predominantly adopts a stable binding pose while occasionally sampling alternative configurations under physiological conditions. The principal component analysis (PCA) was performed to evaluate the conformational variance in the Quinolonimide-SIRT3 system. The first few eigenvectors contributed the most significant portion of the total variance, with PC1 capturing the highest degree of fluctuations (**Fig 11A**). A 2D PCA-based free energy surface was then generated by projecting the simulation data onto PC1 and PC2, revealing two main basins: a predominant low-energy region, where Quinolonimide remained most frequently, and a smaller high-energy state sampled intermittently (**Fig 11B**). The majority of frames were located in the local-minima well, indicating that Quinolonimide largely maintains a stable binding orientation while occasionally exploring alternative conformations under the simulation conditions. In the principal component analyses for Brevianamide R complex, the first three principal components (PC1, PC2, and PC3) accounted for 18.59%, 13.34%, and 9.72% of the total variance, respectively, giving a combined 41.65% coverage of overall conformational fluctuations (**Fig 12A**). PC1 thus showed the most significant motion at 18.59%. Furthermore, a 2D PCA-based free energy surface was generated to pinpoint the thermodynamically stable states, revealing a dominant low-energy basin where the complex spent most of its time, along with a higher-energy region sampled intermittently. This distribution suggests that the system predominantly adopts a stable conformation, with occasional excursions into alternative states (**Fig 12B**). These findings indicate that the system remains largely in a stable conformation while exploring higher-energy states less frequently, suggesting a well-defined, low-energy binding mode with limited but noteworthy conformational flexibility
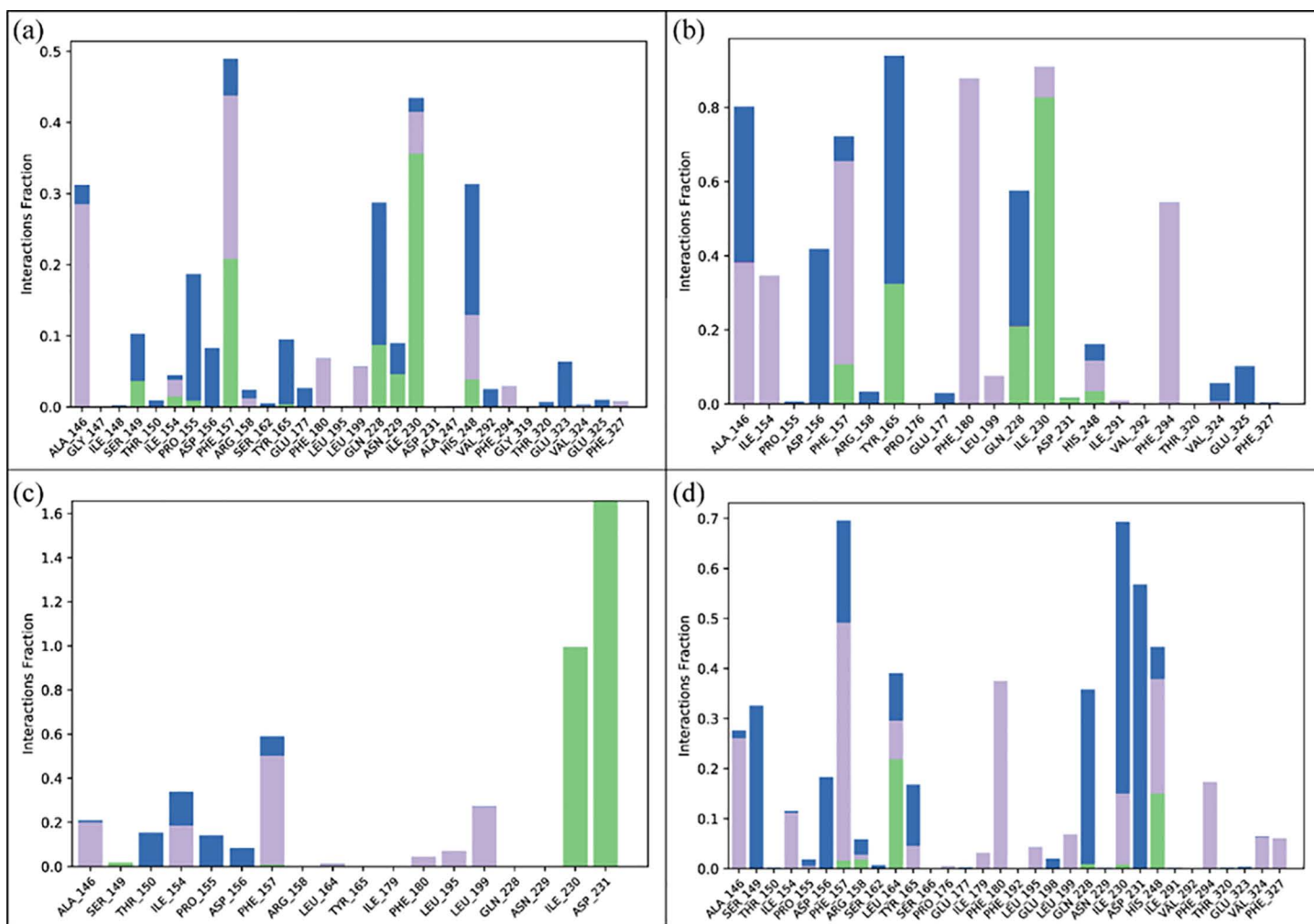
Fig 6. The protein-ligand interactions. (a) Penipanoid C, (b) Penicillactam, (c) Quinolonimide, (d) Brevianamide R. Green bars show hydrogen bonding, gray show hydrophobic interactions, and blue shows the water bridges.

3.5.7. MMGBSA and energy decomposition analyses. The MMGBSA results indicate that the van der Waals (ΔE_{vdW}) and electrostatic (ΔE_{ele}) terms are the primary contributors to binding across all four complexes, whereas the polar solvation energy partially offsets these favorable interactions. Notably, Quinolonimide and Penipanoid C exhibit slightly more negative total free energies (ΔG_{total}), suggesting stronger overall affinity for SIRT3 compared to Penicillactam **C and Brevianamide R. In each case, the negative gas-phase energy (ΔG_{gas}) underscores stable, energetically** favorable interactions in the binding pocket, while the solvation term (ΔG_{solv}) exerts a smaller, unfavorable effect. These findings support the stable binding modes observed in molecular docking and MD simulations, further highlighting the potential of these compounds as SIRT3 inhibitors (**Fig 13**). Per residue energy decomposition analysis reveals that Phe157 consistently provides strong stabilizing interactions across all four complexes. For Penipanoid C, additional key contributions stem from Phe180, Ile230, and His248, reflecting strong hydrophobic and/or π-stacking contacts. Penicillactam likewise shows major energy contributions from Phe157, Phe180, and His248, with a moderate role from Ala146. In Quinolonimide, the largest negative energy values localize around Phe157 and Ile230, highlighting these residues as principal anchoring points. Brevianamide R, on the other hand, exhibits pronounced stabilization from
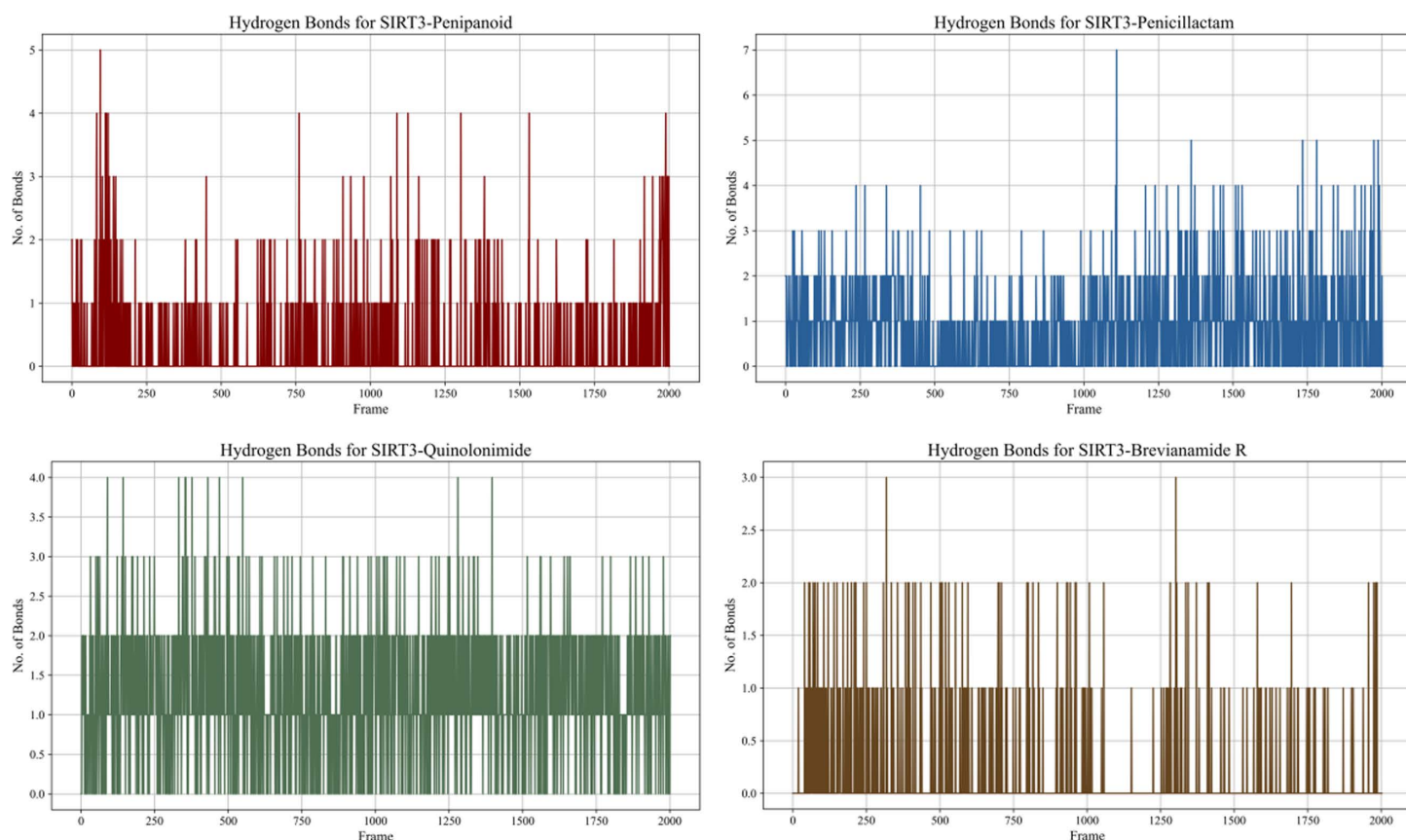
Fig 7. Hydrogen bond formation over time for each SIRT3–ligands complex during the 100 ns MD simulation. Plots (from top-left to bottom-right) show Penipanoid C, Penicillactam, Quinolonimide, and Brevianamide R, respectively. The y-axis indicates the number of hydrogen bonds formed at each simulation frame (x-axis), illustrating how consistently each compound maintains polar contacts with the SIRT3 active site.

https://doi.org/10.1371/journal.pone.0323107.g007

Phe157, His248, and Phe294. These findings underscore the critical role of the aromatic/hydrophobic pocket formed by Phe157, Phe180, Ile230, His248, and Phe294 in ligand binding, corroborating the stable interactions observed in both docking and MD simulations (**Fig 14**) [40].

4. Discussion

SIRT3, the primary deacetylase located within mitochondria, is implicated in various facets of mitochondrial metabolism, encompassing mitochondrial synthesis and movement. Given the critical role of mitochondria in cellular functions, any dysregulation leading to dysfunction can contribute to a wide array of diseases. SIRT3 dysregulation has been associated with different mitochondrial disorders. The amount of evidence that has accumulated over time has gradually revealed the complexities of SIRT3's innate biological functions, providing insight into possible therapeutic uses in human diseases. From its original classification as a gene associated with longevity to its current status as a "superstar" target for the treatment of multiple diseases, SIRT3 has attracted a lot of attention [41,42]. The focus of this study is to explore deep-sea fungal metabolites with the aim of identifying novel inhibitors against SIRT3, contributing to the ongoing efforts to understand and potentially manipulate SIRT3 for therapeutic purposes.

Microbial natural product research has gained prominence owing to the capacity of microorganisms to generate biosynthetically rare, biologically active, and structurally diverse metabolites like their hosts. The advantageous features of large-scale metabolite production without harming hosts, rapid generation, and reproducibility make this area of study
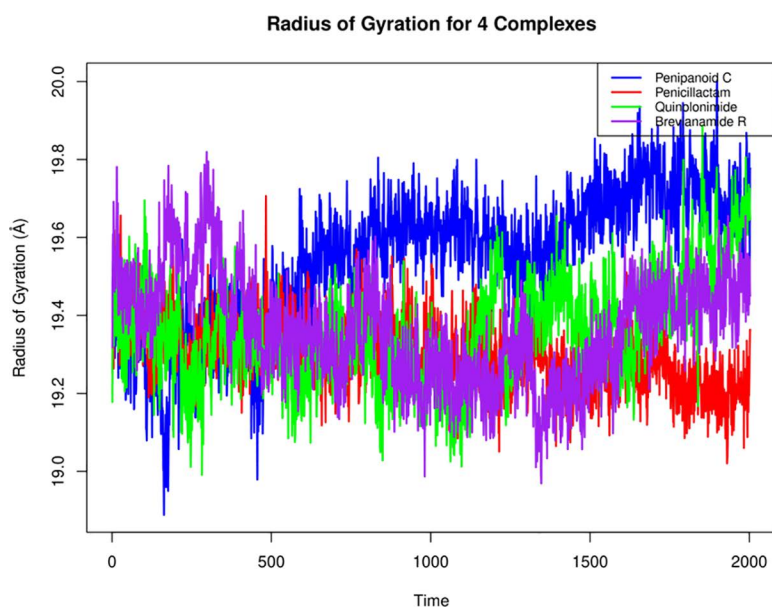
Radius of Gyration for 4 Complexes

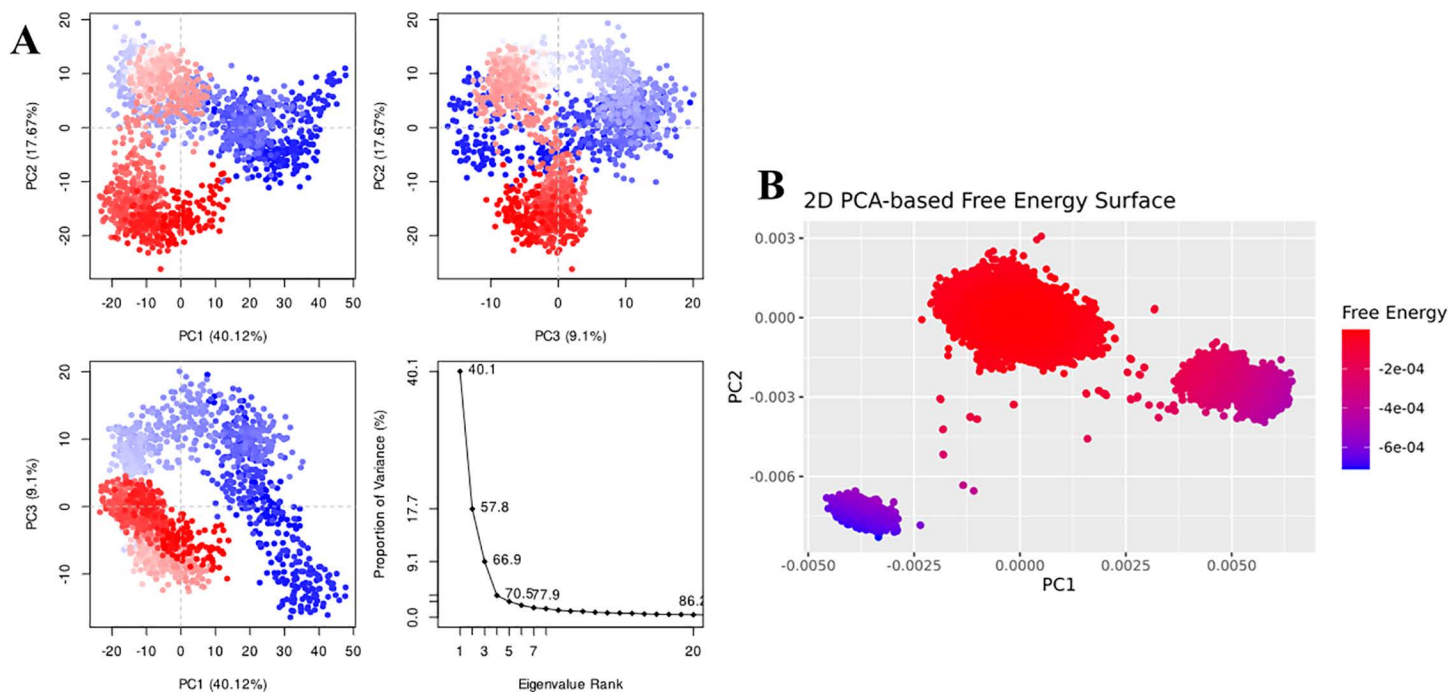**Fig 8. Radius of gyration plot of all four complexes with respect to time.**

Fig 9. (A) The principal component analysis for Penipanoid C complex, indicating the fluctuations in different hyperspaces. (B) PCA based free energy surface of the complex calculated during simulation.
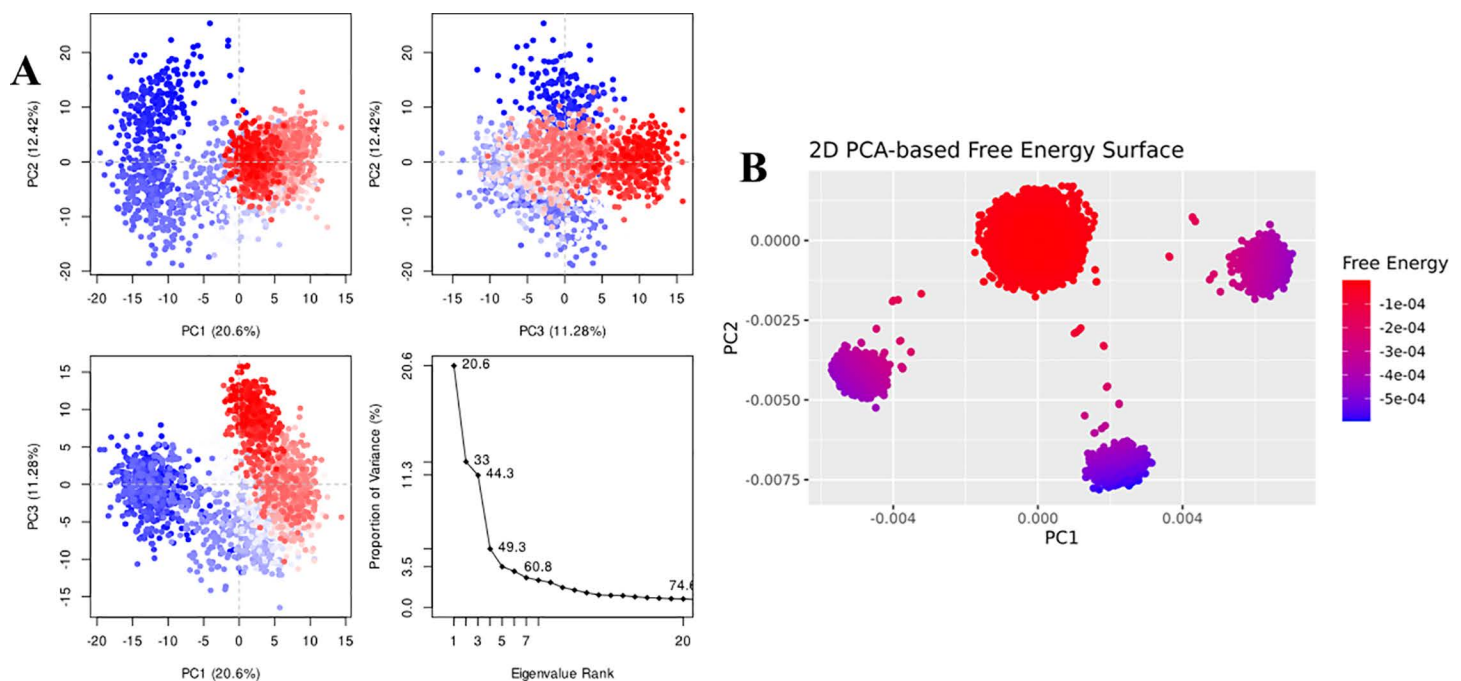
Fig 10. (A) The principal component analysis for Penicilactam complex, indicating the fluctuations in different hyperspaces. (B) PCA based free energy surface of the complex calculated during simulation.

https://doi.org/10.1371/journal.pone.0323107.g010

particularly appealing. As a result, secondary metabolites derived from marine microorganisms exhibit distinctive and diverse structures, coupled with significant biological activities, holding substantial potential for applications in traditional Chinese medicine [43]. Deep-sea fungi have become a focal point for researchers due to their capacity to produce diverse secondary metabolites, high occurrence rates, and notable biological activities within the deep-sea microbial community. The identification of secondary metabolites from marine fungi is increasingly capturing the attention of researchers seeking to develop novel drugs [44,45].

The structures of deep-sea fungal metabolites were obtained from PubChem. The prepared compounds were docked to the prepared SIRT3 receptor to predict binding affinities using the standard precision mode of the glide tool. The computational technique of molecular docking predicts the binding affinity of ligands to receptor proteins. Although it has applications in nutraceutical research, it has evolved into a formidable drug development tool[46,47]. The top ten compounds (Cyclopiamide D, Penilumamide K, Coccoquinone A, Penipanoid C, Penicillactam, Quinolonimide, Prenylterphenyllin, Brevianamide R, Butanolide A, and Dichotocejpin C) were chosen for analysis based on their binding affinities. The binding affinities of the chosen compounds ranged from -9.693 to -8.327 kcal/mol. The binding affinities of the selected compounds suggested that they could inhibit the function of the SIRT3 protein.

The assessment of ADMET characteristics and toxicity risks for the selected compounds revealed predicted values within an acceptable range. Evaluating the ADMET properties is a crucial aspect of the drug development process. It enables the prediction of potential toxicity, behavior, and outcomes of a proposed drug within the human body. Understanding these properties aids in making informed decisions about the safety and efficacy of drug candidates during the development phase [48–50]. Except for Cyclopiamide D, Coccoquinone A, Butanolide A, and Dichotocejpin C, none of the compounds were found to be toxic. Based on the pharmacokinetic and toxicity profiles, four compounds were chosen for molecular interactions analysis Penipanoid C, Penicillactam, Quinolonimide, and Brevianamide R.
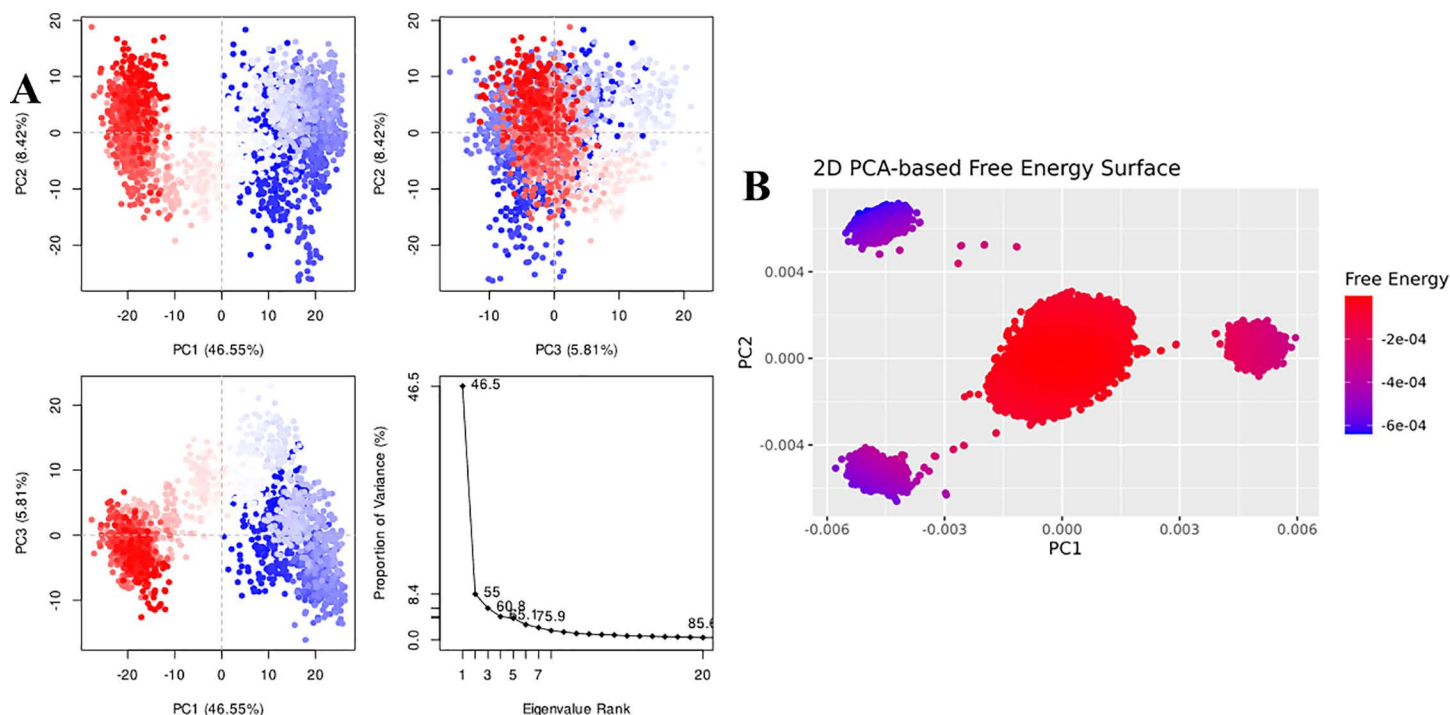
Fig 11. (A) The principal component analysis for Quinolinimide complex, indicating the fluctuations in different hyperspaces. (B) PCA based free energy surface of the complex calculated during simulation.

https://doi.org/10.1371/journal.pone.0323107.g011

After the analysis of the molecular interactions, the compounds that were chosen for analysis were aligned on the co-crystal ligand to determine their binding modes. The plausible binding modes of the four hits were examined with alignment of the co-crystal ligand. Consequently, the aligned modes were subjected to MD simulation for the protein dynamics and structure stability analysis. MD simulations serve as an effective tool for understanding the stability of protein-ligand complexes [51]. The MD simulation analysis suggests that the selected compounds remained stably bound to the target protein.

Researchers can observe the binding process in real time using MD simulations. MD can aid in the identification of potential drug candidates by monitoring the conformational changes of the protein and ligand, the binding pathway, and binding affinities. By offering a more thorough comprehension of the interactions between drug candidates and their target biomolecules, they facilitate the logical design of innovative therapeutics [51,52]. According to MD simulation studies, these compounds were stable as effective inhibitors within the protein binding pocket. Moreover, the hydrogen bonding analysis, radius of gyration, PCA (with its 2D free energy surface), per-residue energy decomposition, and MMGBSA calculations collectively confirm that our selected compounds form stable, energetically favorable interactions within the SIRT3 binding site. These integrated findings strongly support the potential of these deep-sea fungal metabolites as robust lead candidates for further experimental validation and therapeutic development. Overall, our findings underscore the promising potential of deep-sea fungal metabolites as effective modulators of SIRT3, suggesting that these compounds could be further developed into innovative therapeutic agents. Given SIRT3's critical role in maintaining mitochondrial and metabolic homeostasis, these leads represent valuable starting points for new treatments targeting diseases associated with SIRT3 dysregulation.
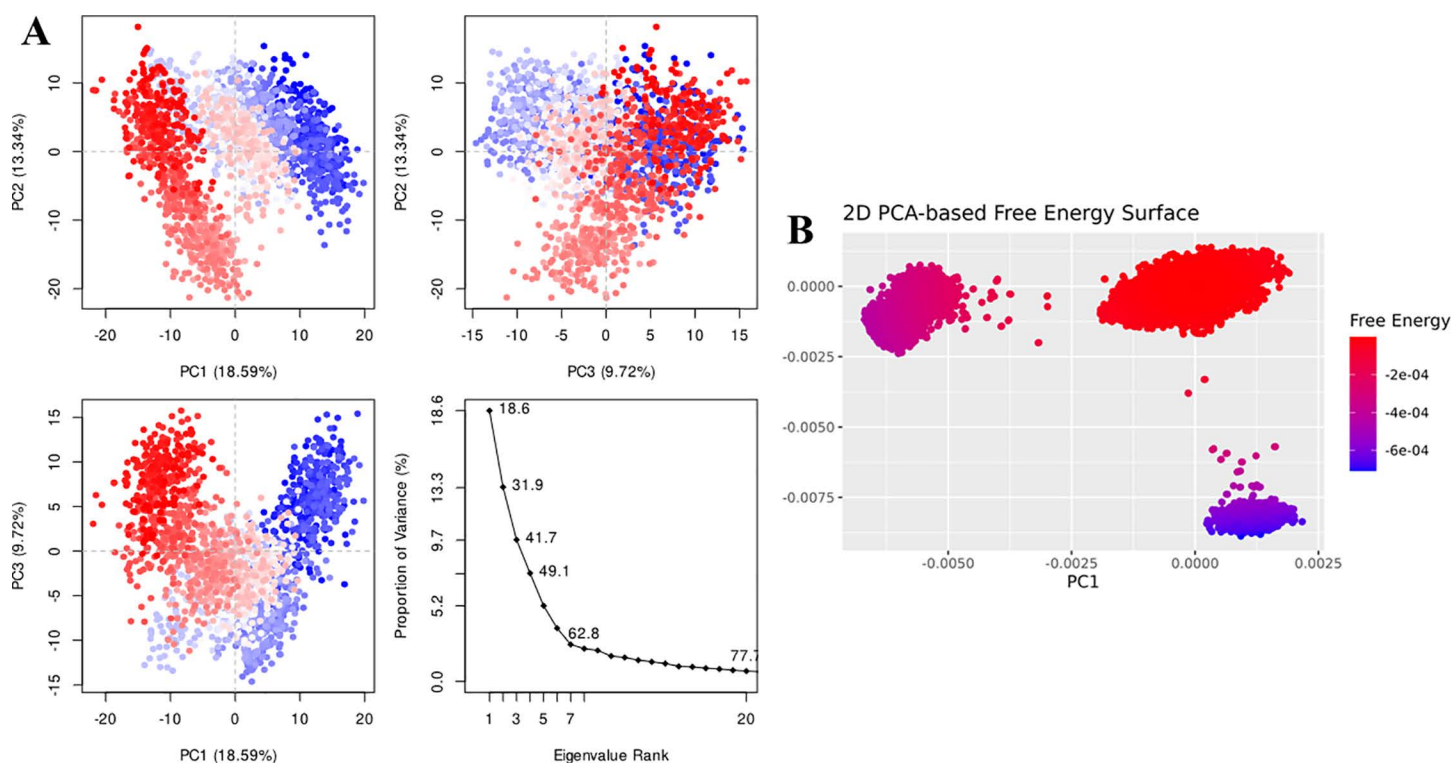
Fig 12. (A) The principal component analysis for Brevianamide R complex, indicating the fluctuations in different hyperspaces. (B) PCA based free energy surface of the complex calculated during simulation.

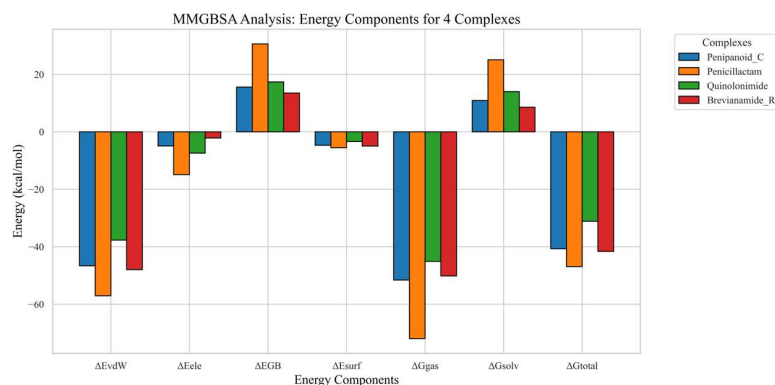https://doi.org/10.1371/journal.pone.0323107.g012

Fig 13. MMGBSA energy component decomposition for the four SIRT3–ligand complexes. Each bar represents a different energy contribution (van der Waals, electrostatic, polar and nonpolar solvation, and total binding energy) to the overall binding affinity. More negative values indicate stronger stabilization.

https://doi.org/10.1371/journal.pone.0323107.g013

Conclusion

In this study, we screened deep sea fungal metabolites for novel SIRT3 inhibitors using molecular docking and ADMET analysis to develop therapeutic interventions. The binding affinities of the screened hits were determined by molecular docking which indicated the strong interactions between ligand and protein. Further, the protein dynamics and
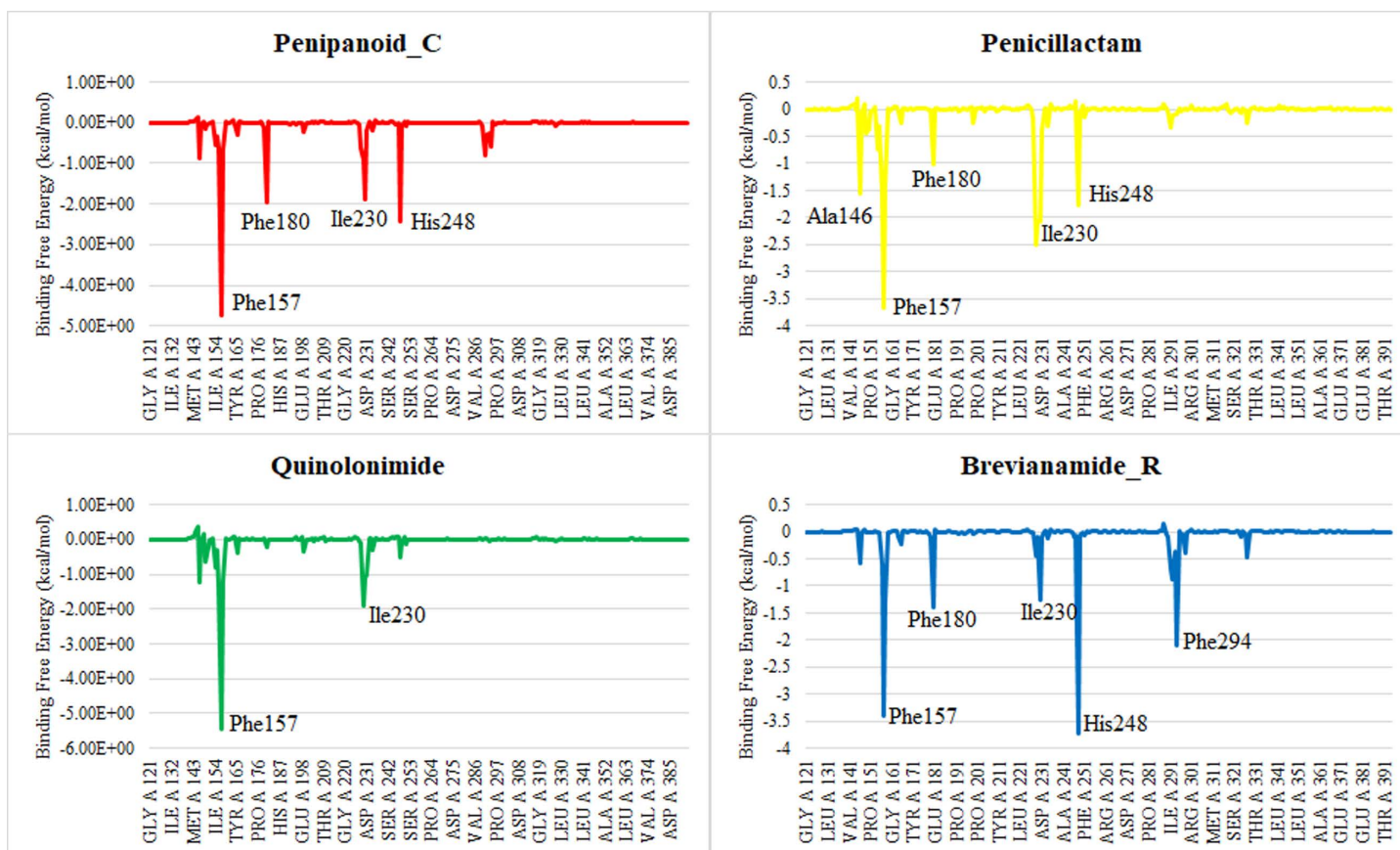
Fig 14. Per residue energy decomposition of the four SIRT3-ligand complexes. Bars below zero (negative values) indicate residues that strongly stabilize ligand binding, while positive values represent unfavorable contributions.

https://doi.org/10.1371/journal.pone.0323107.g014

confirmational changes of the four selected compounds Penipanoid C, Penicillactam, Quinolonimide, and Brevianamide R, were analyzed by MD simulation which showed no major changes in the protein and stability of bound ligands with proteins. This promising outcome underscores the significance of further investigations and validations, both computationally and experimentally, to advance the understanding and development of these compounds as potential therapeutics.

Author contributions

Conceptualization: Abdullah R. Alanzi.

Data curation: Bayan Abdullah Alhaidhal.

Formal analysis: Raghad Mohammad Aloatibi.

Funding acquisition: Abdullah R. Alanzi.

Methodology: Bayan Abdullah Alhaidhal.

Supervision: Abdullah R. Alanzi.

Validation: Raghad Mohammad Aloatibi.

Writing – original draft: Bayan Abdullah Alhaidhal, Raghad Mohammad Aloatibi.

Writing – review & editing: Abdullah R. Alanzi.

References

1. Schwer B, Verdin E. Conserved metabolic regulatory functions of sirtuins. Cell Metab. 2008;7(2):104–12. https://doi.org/10.1016/j.cmet.2007.11.006 PMID: 18249170

2. Zhang J, Xiang H, Liu J, Chen Y, He R-R, Liu B. Mitochondrial sirtuin 3: new emerging biological function and therapeutic target. Theranostics. 2020;10(18):8315–42. https://doi.org/10.7150/thno.45922 PMID: 32724473

3. Wu QJ, et al. The sirtuin family in health and disease. Signal Transduct Target Ther. 2022;7(1):402.

4. Frye RA. Characterization of five human cDNAs with homology to the yeast SIR2 gene: Sir2-like proteins (sirtuins) metabolize NAD and may have protein ADP-ribosyltransferase activity. Biochem Biophys Res Commun. 1999;260(1):273–9. https://doi.org/10.1006/bbrc.1999.0897 PMID: 10381378

5. Zhang Y, Nie L, Xu K, Fu Y, Zhong J, Gu K, et al. SIRT6, a novel direct transcriptional target of FoxO3a, mediates colon cancer therapy. Theranostics. 2019;9(8):2380–94. https://doi.org/10.7150/thno.29724 PMID: 31149050

6. Meng H, Yan W-Y, Lei Y-H, Wan Z, Hou Y-Y, Sun L-K, et al. SIRT3 regulation of mitochondrial quality control in neurodegenerative diseases. Front Aging Neurosci. 2019;11:313. https://doi.org/10.3389/fnagi.2019.00313 PMID: 31780922

7. Samant SA, Zhang HJ, Hong Z, Pillai VB, Sundaresan NR, Wolfgeher D, et al. SIRT3 deacetylates and activates OPA1 to regulate mitochondrial dynamics during stress. Mol Cell Biol. 2014;34(5):807–19. https://doi.org/10.1128/MCB.01483-13 PMID: 24344202

8. Papa L, Germain D. Correction for Papa and Germain, "SirT3 regulates a novel arm of the mitochondrial unfolded protein response". Mol Cellular Biol. 2017.

9. Jin L, Galonek H, Israelian K, Choy W, Morrison M, Xia Y, et al. Biochemical characterization, localization, and tissue distribution of the longer form of mouse SIRT3. Protein Sci. 2009;18(3):514–25. https://doi.org/10.1002/pro.50 PMID: 19241369

10. Zhao J, Liu Y, Zhu L, Li J, Liu Y, Luo J, et al. Tumor cell membrane-coated continuous electrochemical sensor for GLUT1 inhibitor screening. J Pharm Anal. 2023;13(6):673–82. https://doi.org/10.1016/j.jpha.2023.04.015 PMID: 37440905

11. Verdin E, Hirschey MD, Finley LWS, Haigis MC. Sirtuin regulation of mitochondria: energy production, apoptosis, and signaling. Trends Biochem Sci. 2010;35(12):669–75. https://doi.org/10.1016/j.tibs.2010.07.003 PMID: 20863707

12. Zhang Y, Wen P, Luo J, Ding H, Cao H, He W, et al. Sirtuin 3 regulates mitochondrial protein acetylation and metabolism in tubular epithelial cells during renal fibrosis. Cell Death Dis. 2021;12(9):847. https://doi.org/10.1038/s41419-021-04134-4 PMID: 34518519

13. Zhang J, et al. Mitochondrial Sirtuin 3: new emerging biological function and therapeutic target. Theranostics. 2020;10(18):8315.

14. Lu J, Zhang H, Chen X, Zou Y, Li J, Wang L, et al. A small molecule activator of SIRT3 promotes deacetylation and activation of manganese superoxide dismutase. Free Radic Biol Med. 2017;112:287–97. https://doi.org/10.1016/j.freeradbiomed.2017.07.012 PMID: 28711502

15. Pillai VB, Samant S, Sundaresan NR, Raghuraman H, Kim G, Bonner MY, et al. Honokiol blocks and reverses cardiac hypertrophy in mice by activating mitochondrial Sirt3. Nat Commun. 2015;6:6656. https://doi.org/10.1038/ncomms7656 PMID: 25871545

16. Upadhyay A, et al. Nonallosteric sirtuin enzyme activation: characterization of hit compounds biorxiv 2020 p. 2020.04.17.045187.

17. Jiang M, Chen S, Lu X, Guo H, Chen S, Yin X, et al. Integrating genomics and metabolomics for the targeted discovery of new cyclopeptides with antifungal activity from a marine-derived fungus Beauveria felina. J Agric Food Chem. 2023;71(25):9782–95. https://doi.org/10.1021/acs.jafc.3c02415 PMID: 37310400

18. LigPrep L. Schrödinger, LLC.; 2018.

19. Shivakumar D, Harder E, Damm W, Friesner RA, Sherman W. Improving the prediction of absolute solvation free energies using the next generation OPLS force field. J Chem Theory Comput. 2012;8(8):2553–8. https://doi.org/10.1021/ct300203w PMID: 26592101

20. Schrödinger, L.J.S.S. Schrödinger, LLC; New York, NY: 2017. p. 2.

21. Kim MO, Nichols SE, Wang Y, McCammon JA. Effects of histidine protonation and rotameric states on virtual screening of *M. tuberculosis* RmlC. J Comput Aided Mol Des. 2013;27(3):235–46. https://doi.org/10.1007/s10822-013-9643-9 PMID: 23579613

22. Rostkowski M, et al. Graphical analysis of pH-dependent properties of proteins predicted using PROPKA. 2011;11(1):1–6.

23. Friesner RA, Banks JL, Murphy RB, Halgren TA, Klicic JJ, Mainz DT, et al. Glide: a new approach for rapid, accurate docking and scoring. 1. Method and assessment of docking accuracy. J Med Chem. 2004;47(7):1739–49. https://doi.org/10.1021/jm0306430 PMID: 15027865

24. Agamah FE, Mazandu GK, Hassan R, Bope CD, Thomford NE, Ghansah A, et al. Computational/in silico methods in drug target and lead prediction. Brief Bioinform. 2020;21(5):1663–75. https://doi.org/10.1093/bib/bbz103 PMID: 31711157

25. Oduselu GO, et al. Homology modelling and molecular docking studies of selected substituted benzo [d] imidazol-1-yl) methyl) benzimidamide scaffolds on Plasmodium falciparum adenylosuccinate lyase receptor. 2019;13:1177932219865533.

26. Osiris. Osiris Property Explorer. [cited Dec 25, 2024] Available from: https://www.organic-chemistry.org/prog/peo/.

27. Bowers KJ, et al. Scalable algorithms for molecular dynamics simulations on commodity clusters. Proceedings of the 2006 ACM/IEEE Conference on Supercomputing. 2006

28. Price DJ, Brooks CL 3rd. A modified TIP3P water potential for simulation with Ewald summation. J Chem Phys. 2004;121(20):10096–103. https://doi.org/10.1063/1.1808117 PMID: 15549884

29. Kumari R, Rathi R, Pathak SR, Dalal V. Computational investigation of potent inhibitors against YsxC: structure-based pharmacophore modeling, molecular docking, molecular dynamics, and binding free energy. J Biomol Struct Dyn. 2023;41(3):930–41. https://doi.org/10.1080/07391102.2021.2015446 PMID: 34913841

30. Goodnow Jr R. Small molecule lead generation processes for drug discovery. Drugs Future. 2002;27(12)

31. Husain A, Ahmad A, Khan SA, Asif M, Bhutani R, Al-Abbasi FA. Synthesis, molecular properties, toxicity and biological evaluation of some new substituted imidazolidine derivatives in search of potent anti-inflammatory agents. Saudi Pharm J. 2016;24(1):104–14. https://doi.org/10.1016/j.jsps.2015.02.008 PMID: 26903774

32. Gogoi P, et al. In silico study, synthesis, and evaluation of the antimalarial activity of hybrid dimethoxy pyrazole 1, 3, 5-triazine derivatives. 2021;35(3):e22682.

33. Behrouz S, Soltani Rad MN, Taghavi Shahraki B, Fathalipour M, Behrouz M, Mirkhani H. Design, synthesis, and in silico studies of novel eugenyloxy propanol azole derivatives having potent antinociceptive activity and evaluation of their β-adrenoceptor blocking property. Mol Divers. 2019;23(1):147–64. https://doi.org/10.1007/s11030-018-9867-7 PMID: 30094501

34. Thillainayagam M, Malathi K, Ramaiah S. In-Silico molecular docking and simulation studies on novel chalcone and flavone hybrid derivatives with 1, 2, 3-triazole linkage as vital inhibitors of Plasmodium falciparum dihydroorotate dehydrogenase. J Biomol Struct Dyn. 2018;36(15):3993–4009. https://doi.org/10.1080/07391102.2017.1404935 PMID: 29132266

35. Sargsyan K, Grauffel C, Lim C. How molecular size impacts RMSD applications in molecular dynamics simulations. J Chem Theory Comput. 2017;13(4):1518–24. https://doi.org/10.1021/acs.jctc.7b00028 PMID: 28267328

36. Dhankhar P, Dalal V, Singh V, Tomar S, Kumar P. Computational guided identification of novel potent inhibitors of N-terminal domain of nucleocapsid protein of severe acute respiratory syndrome coronavirus 2. J Biomol Struct Dyn. 2022;40(9):4084–99. https://doi.org/10.1080/07391102.2020.1852968 PMID: 33251943

37. Martínez L. Automatic identification of mobile and rigid substructures in molecular dynamics simulations and fractional structural fluctuation analysis. PLoS One. 2015;10(3):e0119264. https://doi.org/10.1371/journal.pone.0119264 PMID: 25816325

38. Ashraf N, et al Combined 3D-QSAR, molecular docking and dynamics simulations studies to model and design TTK inhibitors. 2022;10.

39. Alanzi A.R. et al. Molecular docking and ADMET studies of halogenated metabolites from marine sponges as inhibitors of wild-type and mutants PBP2 in Neisseria gonorrhoeae. 2023;1–13.

40. Halder D, Das S, Jeyaprakash RJMD. Identification of natural product as selective PI3Kα inhibitor against NSCLC: multi-ligand pharmacophore modeling, molecular docking, ADME, DFT, and MD simulations. 2023:1–28.

41. Reverdy C, Gitton G, Guan X, Adhya I, Krishna Dumpati R, Roy S, et al. Discovery of novel compounds as potent activators of Sirt3. Bioorg Med Chem. 2022;73:116999. https://doi.org/10.1016/j.bmc.2022.116999 PMID: 36191547

42. Kanwal A. Functional and therapeutic potential of mitochondrial SIRT3 deacetylase in disease conditions. Expert Rev Clin Pharmacol. 2018;11(12):1151–5. https://doi.org/10.1080/17512433.2018.1546119 PMID: 30427218

43. Yin Q, et al. Chemistry and bioactivities of alkaloids isolated from marine fungi (covering 2016–2022). Fitoterapia 2022:105377.

44. Wang Z, et al. Progress in the discovery of new bioactive substances from deep-sea associated fungi during 2020-2022. Front Marine Sci. 2023.

45. Gozari M, Alborz M, El-Seedi HR, Jassbi AR. Chemistry, biosynthesis and biological activity of terpenoids and meroterpenoids in bacteria and fungi isolated from different marine habitats. Eur J Med Chem. 2021;210:112957. https://doi.org/10.1016/j.ejmech.2020.112957 PMID: 33160760

46. Sethi A et al. Molecular docking in modern drug discovery: principles and recent applications. Drug Discovery Development-New Adv. 2019;2:1–21.

47. Stanzione F, Giangreco I, Cole JC. Use of molecular docking computational tools in drug discovery. Prog Med Chem. 2021;60:273–343. https://doi.org/10.1016/bs.pmch.2021.01.004 PMID: 34147204

48. Lin B, He S, Yim HJ, Liang TJ, Hu Z. Evaluation of antiviral drug synergy in an infectious HCV system. Antivir Ther. 2016;21(7):595–603. https://doi.org/10.3851/IMP3044 PMID: 27035622

49. Tsaioun K, Bottlaender M, Mabondzo A. ADDME–Avoiding Drug Development Mistakes Early: central nervous system drug discovery perspective. BMC Neurol. 2009;9(1):1-11.

50. Hardy JA, Higgins GA. Alzheimer's disease: the amyloid cascade hypothesis. Science. 1992;256(5054):184–5. https://doi.org/10.1126/science.1566067 PMID: 1566067

51. Salo-Ahen OMH, Alanko I, Bhadane R, Bonvin AMJJ, Honorato RV, Hossain S, et al. Molecular Dynamics Simulations in Drug Discovery and Pharmaceutical Development. Processes. 2020;9(1):71. https://doi.org/10.3390/pr9010071

52. Shaker B, Ahmad S, Lee J, Jung C, Na D. In silico methods and tools for drug discovery. Comput Biol Med. 2021;137:104851. https://doi.org/10.1016/j.compbiomed.2021.104851 PMID: 34520990